35th Annual International Conference of the IEEE EMBS
Osaka, Japan, 3 - 7 July, 2013

Robust Filtering Based Segmentation and Analysis of Dura Mater Vasculature using Epifluorescence Microscopy

V. B. Surya Prasath[1], F. Bunyak[1], O. Haddad[1], O. V. Glinskii[2,4,5], V. V. Glinsky[3,4,5]
V. H. Huxley[2,4], K. Palaniappan[1]

Abstract— **We show that an adaptive robust filtering based image segmentation model can be used for microvasculature network detection and quantitative characterization in epifluorescence-based high resolution images. Inhomogeneous fluorescence contrast due to the variable binding properties of the lectin marker and leakage hampers accurate vessel segmentation. We use a robust adaptive filtering approach to remove noise and reduce inhomogeneities without destroying small scale vascular structures. An adaptive variance based thresholding method combined with morphological filtering yields an effective detection and segmentation of the vascular network suitable for medial axis estimation. Quantitative parameters of the microvascular network geometry, including curvature, tortuosity, branch segments and branch angles are computed using post segmentation-based medial axis tracing. Experiments using epifluorescence-based high resolution images of porcine and murine microvasculature demonstrates the effectiveness of the proposed approach for quantifying morphological properties of vascular networks.**

I. INTRODUCTION

Vessel extraction, tracing and measurement are important image processing stages for clinically characterizing the behavior of tissue function in normal and diseased states. Various techniques exist in the literature for extracting vessels in neurological, cardiovascular, and ocular imaging. Among them, multi-scale Hessian, structure tensor or eigen analysis and segmentation based approaches are very popular [1]. For example, Zhou et al [2] use a ridge scan-conversion deformable model and a bifurcation detection approach [3] for boundary extraction in CT lung images, Lam and Yan [4] use a divergence vector field scheme for retinal vessel extraction. In fluorescence microscopy imaging, 3D vessel extraction using a GPU implementation is proposed in [5]. A shape-based geodesic active contour scheme is studied in [6] using a Hessian-based initialization level set approach.

Fluorescent imaging techniques are becoming critical techniques for visualizing and analyzing dynamic biological processes, which benefits from the development of new fluorophore-based labeling methods and the development of sophisticated algorithms for the analysis of light microscope imagery. In epifluorescence imaging labeled SBA lectin or WGA lectin is used to stain microvascular structures followed by high resolution fluorescence microscopy. The application of interest here is to automatically extract the structural components of the microvascular system with certain accuracy from images acquired by fluorescence microscopy [7]. Due to uneven contrast, leakage, and high variance in foreground (vessel) intensity, traditional global thresholding schemes [8] can fail to accurately detect salient microvasculature structures. The majority of active contour models [9], [10], [11], [12], [13] typically rely on edge- or region-based indicators, and such schemes may not capture all of the vascular network structures present in a given epifluorescence image. Thus, current approaches to vessel segmentation lead to poor results when applied to epifluorescence imagery of the microvasculature. Hence, a robust denoising process can be beneficially incorporated into the segmentation process in order to extract accurate morphological information.

In order to preserve important structures in the segmentation of the vascular network images such as narrow and low-contrast branches, we utilize an adaptive filtering scheme derived from edge preserving filtering [14], [11] and robust statistics theory [15] along with a local-variance based thresholding step. Such edge-preserving smoothing is related to the well-known anisotropic diffusion filters [16], [17] and bilateral filters [18], see [19]. We derive an improved numerical scheme in the context of robust estimation with emphasis on edge preservation aimed at avoiding local minima problems, which often arise in the context of nonlinear smoothing [20], [21]. The proposed approach provides favorable smoothing results, and its application to microvasculature network structure extraction illustrates the applicability of the method in the field of nanoscale imaging. We present a semiautomated computer-assisted quantitative assessment of microvascular structure from dura mater images which offers a measurable approach to assess microcirculation changes. These studies can be used to understand the physiological and molecular mechanisms leading to gender dependent pathological conditions.

The major contributions of our work include novel combinations of (a) a robust local filtering model with edge preserving properties, and (b) vascular network morphology detection from the smoothed image for further analysis. The rest of the paper is organized as follows. Section II presents the proposed smoothing based microvasculature network detection including the pre- and post- processing steps. Section III describes the vessel network graph extraction and defines the quantitative measures. Section IV provides experimental segmentation results and quantitative analysis of extracted microvasculature networks.

Authors are with the University of Missouri-Columbia, Columbia, MO 65211 USA, [1]Department of Computer Science, [2]Department of Medical Pharmacology and Physiology, [3]Department of Pathology and Anatomical Sciences, [4]National Center for Gender Physiology, and [5]Research Service, Harry S. Truman Memorial Veterans Hospital, Columbia, MO 65201 USA.

978-1-4577-0216-7/13/$26.00 ©2013 European Union

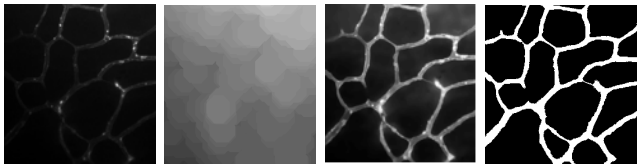

(a) (b) (c) (d)

Fig. 1. Illustration of the smoothing and microvasculature extraction steps on an epifluorescence image taken from a Yucatan miniature swine. (a) Input image (b) Estimated background using top-hat transformation (4) (c) Background subtracted and filtered image u by running scheme (3) for $T = 5$ iterations (d) Adaptive thresholding with Niblack's scheme after post processing with morphological opening and closing to remove outliers.

II. ROBUST SMOOTHING BASED VASCULATURE DETECTION

Let $\Omega \subset \mathbb{R}^2$ be the image domain, typically a rectangle and the input image $I : \Omega \to \mathbb{R}$ with $I(\mathbf{x})$ represents the value at a pixel $\mathbf{x} \in \Omega$. In a robust statistics framework finding a best fit of a smooth image u from a given noisy input image I can be posed as a minimization problem [14],

$$\min_u \left\{ \sum_{\mathbf{x}\in\Omega} \sum_{\mathbf{y}\in\mathcal{N}_\mathbf{x}} \omega(\mathbf{x}-\mathbf{y})\rho(I(\mathbf{x})-u(\mathbf{x}),\sigma) \right\} \tag{1}$$

with a robust estimator function ρ. Here $\mathcal{N}_\mathbf{x}$ represents the neighborhood of a pixel $\mathbf{x}$, ω is a spatial weighting function (e.g. Gaussian kernel) and σ is the scale (variance) parameter. Among a wide variety of choices for the robust norm, ρ, in this paper we use Tukey's biweight robust function due its strong edge preserving property. To solve the minimization problem (1) we use the dilation convex approximation [14] of the Tukey function,

$$\rho_\gamma(\xi,\sigma) = \begin{cases} \frac{\gamma^2\sigma^2}{6}(1-[1-(\xi/\gamma\sigma)^2]^3) & |\xi| \le \gamma\sigma, \\ 1/3 & \text{otherwise.} \end{cases} \tag{2}$$

Here $\gamma > 0$ is the dilation parameter. We use an iterative reweighted method to solve (1) [14],

$$u_\mathbf{y}^{t+1} = \frac{\sum_{\mathbf{x}\in\mathcal{N}_\mathbf{y}} \omega(\mathbf{x}-\mathbf{y})c(I(\mathbf{x})-u^t(\mathbf{y}))I(\mathbf{x})}{\sum_{\mathbf{x}\in\mathcal{N}_\mathbf{y}} \omega(\mathbf{x}-\mathbf{y})c(I(\mathbf{x})-u^t(\mathbf{y}))} \tag{3}$$

where $c(\xi) = \rho'_\gamma(\xi)/\xi$ and t iteration number. Then, our micro-vessel extraction routine consists of the following four sequential steps.

1) Pre-processing: Using the morphological top-hat operator to estimate the inhomogeneous background present in epifluorescence images,

$$\text{tophat}(I) = I - ((I \ominus SE) \oplus SE) \tag{4}$$

where $(I \ominus SE)(\tilde{\mathbf{x}}) = \min\{I(\mathbf{x}+\tilde{\mathbf{x}}) + SE(\mathbf{x})\}$ and $(I \oplus SE)(\tilde{\mathbf{x}}) = \max\{I(\mathbf{x}+\tilde{\mathbf{x}}) + SE(\mathbf{x})\}$ define the opening with structuring element SE with $\tilde{\mathbf{x}} \in \mathcal{N}_\mathbf{x}$, a neighborhood of $\mathbf{x}$, see Figure 1(b) where the estimated background from a given image is shown.
2) Robust image filtering: Running the proposed robust smoothing algorithm in (1) on the enhanced image, see Figure 1(c).
3) Adaptive thresholding algorithm: Niblack's thresholding algorithm [22] which is based on the local mean and variance values.
4) Post-processing: Using morphological opening and closing to remove small outlier regions to obtain the segmentation mask M_{vessel}, see Figure 1(d).

We observe in Figure 1(c) that noise and inhomogeneous subregions are effectively removed in the resulting image after the adaptive smoothing step. Moreover, the major parts of vasculature are accurately preserved in the detection step, see Figure 1(d), such as some narrow and low-contrast branches; see also Figure 2(b) for more examples. Next, we describe the network graph extraction module and quantitative parameters computed using the graph.

III. VESSEL NETWORK GRAPH EXTRACTION AND QUANTITATIVE MEASUREMENTS

This module constructs a vessel network graph by computing the skeleton/medial axis (using thinning procedures as in [23]) from segmentation results obtained using preprocessing and the segmentation module described in the previous section. Further quantitative analysis is performed on the resulting labeled vessel branches.

Step 1: Skeleton (medial axis) $\mathcal{S}_{vessel}$ is extracted from vessel mask $\mathrm{M_{vessel}}$.
Step 2: Branching/bifurcation points $\mathcal{B}_{vessel}$ in $\mathcal{S}_{vessel}$ are identified.
Step 3: Skeleton $\mathcal{S}_{vessel}$ is disconnected at branch points. Connected component labeling is applied to the set of branch points $\mathcal{B}_{vessel}$ and disconnected vessel skeleton $\mathcal{S}_{vessel}$ resulting in uniquely labeled branching points $\mathcal{B} = \{b_1, b_2, ..., b_m\}$ and skeleton segments $\mathcal{S} = \{s_1, s_2, ...s_n\}$.
Step 4: A vessel network graph $G = (\mathcal{S}, \mathcal{B}, E)$ is constructed using branch points $\mathcal{B}$ and skeleton segments $\mathcal{S}$ as vertices in G. Each connected branch point b_i and segment s_j are topologically linked using an edge E_{ij}.
Step 5: Short skeleton segments associated with spurs are removed and corresponding branch points are updated.
Step 6: For each branch point b_i, the set of incident skeleton segments $\mathcal{S}_i = \{s_{i,1}, s_{i,2}, ..\}$ are identified.
Step 7: Labeled skeleton segments $\mathcal{S}_i = \{s_{i,1}, s_{i,2}, ..\}$ are traced and corresponding parametric curves are obtained, $\mathcal{S}(s) = (x(s), y(s))$.

The major skeleton segments are used to obtain the following quantitative measures characterizing the microvascular network.

1) **Vessel Curvature**

$$\begin{aligned} \kappa &= \frac{\dot{x}\ddot{y} - \dot{y}\ddot{x}}{(\dot{x}^2+\dot{y}^2)^{3/2}} \\ &= \frac{(x_p - x_{p-1})(y_{p+1} - 2y_p + y_{p-1})}{(\sqrt{(x_p-x_{p-1})^2 + (y_p-y_{p-1})^2})^3} \\ &\quad - \frac{(y_p - y_{p-1})(x_{p+1} - 2x_p + x_{p-1})}{(\sqrt{(x_p-x_{p-1})^2 + (y_p-y_{p-1})^2})^3} \end{aligned} \tag{5}$$

where the dot refers to derivatives with respect to parameter s. The second expression gives the central

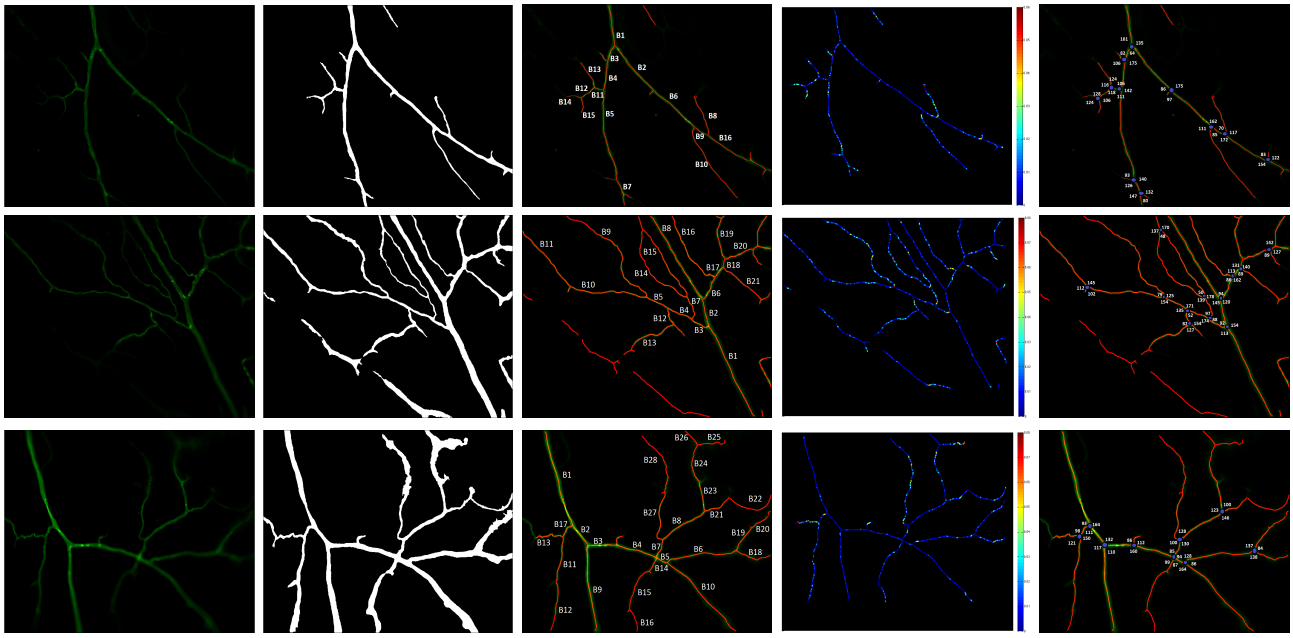

(a) (b) (c) (d) (e)

Fig. 2. Segmentation, medial axis and quantitative parameter estimation results for images taken from three different mice exhibiting varying characteristics; row 1 (Mouse 1 - 012606ERbWT14), row 2 (Mouse 2 - 012706ERbKO15b), row 3 (Mouse 3 - 100605ERbKO14). (a) Original epifluorescence images stained using a green fluorescence marker. (b) Final segmentation mask obtained using the scheme outlined in Section II. (c) Medial axis (red channel) computed using the segmentation mask and superimposed on the original image (green channel) with segments labeled. (d) Quantitative curvature image computed using medial axes and extracted network graphs. (e) Automatically detected branch points and associated branch angles (in degrees).

differences formula for the derivatives involved. Figure 2(d) shows the unsigned curvature map $|\kappa|$, for each of the images highlighting the geometry of the vascular network for three distinct cases.

2) **Vessel tortuosity**

$$\tau = \frac{\text{Arc length}}{\text{Chord}} = \frac{\int_0^l \sqrt{\left(\frac{dx}{ds}\right)^2 + \left(\frac{dy}{ds}\right)^2}\, ds}{\sqrt{(x_0 - x_l)^2 + (y_0 - y_l)^2}} \qquad (6)$$

where *arc length* is the arc length computed from parametric vessel segment curve $\mathcal{S}(s)$ and *chord* is calculated using the Euclidean distance between the end points of $\mathcal{S}$. Normal vessels are generally smooth and remain straight for low tortuosity values, whereas increased tortuosity results from vascular changes associated with hypertension. Figure 3 show the normalized histograms of tortuosity values for all the branches. These correspond to the branches marked in three different images given in Figure 2(c).

3) **Branching angles** We compute the angle (in degrees) between two daughter vessels using tangent lines at branching points. Branching angle is often related to blood flow efficiency. Low angles are associated with hypertension whereas increased angles have been related to decreased blood flow. In Figure 2(e) we show the computed branch angles at the main bifurcation points superimposed on the input images.

IV. EXPERIMENTAL RESULTS

The main motivation is to investigate the influence of sex hormones on angiogenesis as well as vasculature remodeling in murine and porcine brain dura mater. The endothelial cells were stained using AlexaFluor 488 fluorescently labeled SBA lectin for pig and WGA lectin for mouse laminae respectively, to yield a high contrast image of the vascular walls (foreground) and low intensity avascular background.

The experiments are performed on epifluorescence-based high resolution images of dura mater microvasculature acquired using a video microscopy system (Laborlux 8 microscope from Leitz Wetzlar, Germany) equipped with 75 watt xenon lamp and QICAM high performance digital CCD camera (Quantitative Imaging Corporation, Burnaby, Canada) at 0.56 micron per pixel resolution and image dimensions 1360×1036 pixels.

The robust smoothing based segmentation scheme and the quantitative vascular network parameter estimation algorithms were implemented in Matlab. To implement the relaxed minimization scheme (1), we further use an adaptive logarithmic decrease for the scaling parameter γ of dilated Tukey biweight function (2), $\gamma^t = \gamma^{(0)} + ln(t+1)(1 - \gamma^{(0)})/ln(T+1)$, for $t = 0, 1, \ldots, T$ with maximum iteration set to $T = 5$. The neighborhood $\mathcal{N}_{\mathbf{x}}$ in the iterative scheme (3) is fixed at the size of 9×9 which is found to give better results for our dataset. The scale in (2) is fixed using the mean absolute deviation criteria,

$$\sigma = 1.4826 \times \text{median}(|\nabla I| - \text{median}(|\nabla I|)). \qquad (7)$$

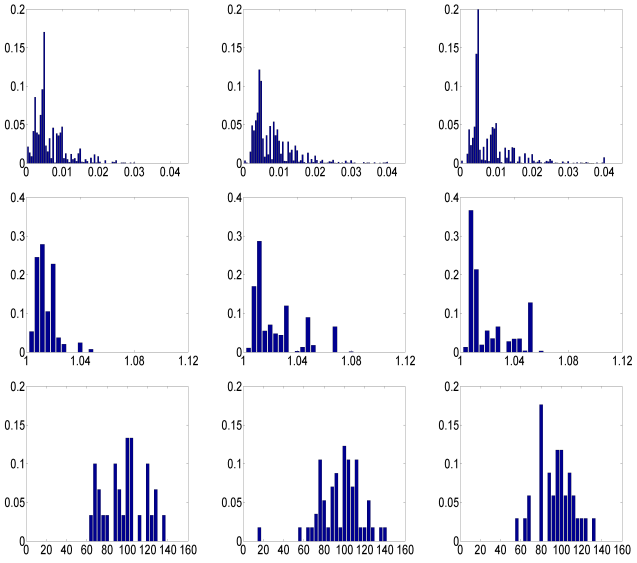

(a) Mouse 1 - 012606ERbWT14 (b) Mouse 2 - 012706ERbKO15b (c) Mouse 3 - 100605ERbKO14

Fig. 3. Normalized histograms showing the distribution of local point-wise curvature (row 1), branch segment based tortuosity (row 2), and branching angles (row 3) for three images shown in Figure 2.

Figure 2 shows some sample segmentation results along with medial axis analysis using our laminae extraction routine described in Section II. As can be seen the segmentation results capture the microvasculature networks and provide a well-defined mask for finding the medial axis, see Figure 2(b). The medial axis is extracted from the segmentation binary mask using morphological thinning and is cleaned for small spurs. Figure 3 shows the normalized histograms of the distribution of local point-wise curvature (row 1), branch segments based tortuosity (row 2), and branching angles (row 3) respectively for the three images shown in Figure 2(a).

V. CONCLUSIONS

We study a scheme for microvasculature detection in epifluorescence images using a robust smoothing model along with adaptive thresholding to obtain a foreground-background segmentation. The robust noise resistant edge preserving smoothing filter proposed in [14] is adapted for the segmentation stage of obtaining vascular network graphs in the presence of background fluorescence response (noise) and inhomogeneous fluorescence labeling. Experimental results on murine dura mater epifluorescence images show promising segmentation results. We extract the medial axis network graph of the microvasculature segmentation in order to estimate quantitative parameters such as curvature, tortuosity and branch points. The proposed automatic segmentation and vascular network quantification software tool will be used for studying ovary excised versus normal intact cases in animal models to understand the systemic influence of hormone therapy on angiogenesis and vascular remodeling. Further studies are being planned to determine the relationships between microvascular morphological changes, disease states, and effects of therapeutic interventions.

ACKNOWLEDGEMENT

This work was partially supported by NIH 5R01 HL078816 and R33 EB00573. Dennis Lubahn kindly provided test animals for the experiments.

REFERENCES

[1] C. Kirbas and F. Quek, "A review of vessel extraction techniques and algorithms," *ACM Comput. Surveys*, vol. 36, no. 2, pp. 81–121, 2004.

[2] J. Zhou, S. Chang, D. Metaxas, and L. Axel, "Vessel boundary extraction using ridge scan-conversion deformable model," in *IEEE ISBI*, 2006, pp. 189–192.

[3] J. Zhou, S. Chang, D. Metaxas, and L. Axel, "Vascular structure segmentation and bifurcation detection," in *IEEE ISBI*, 2007, pp. 872–875.

[4] B. S. Y. Lam and H. Yan, "A novel vessel segmentation algorithm for pathological retina images based on the divergence of vector fields," *IEEE Trans. Medical Imaging*, vol. 27, no. 2, pp. 237–246, 2008.

[5] A. Narayanaswamy et al., "Robust adaptive 3-D segmentation of vessel laminae from fluorescence confocal microscope images and parallel GPU implementation," *IEEE Trans. Medical Imaging*, vol. 29, no. 3, pp. 583–597, 2010.

[6] F. Bunyak et al., "Epifluorescence-based quantitative microvasculature remodeling using geodesic level-sets and shape-based evolution," in *IEEE EMBS*, 2008, pp. 3134–3137.

[7] O. V. Glinskii et al., "Microvascular network remodeling in dura mater of ovariectomized pigs: Role for angiopoietin-1 in estrogen-dependent control of vascular stability," *Am J Physiology*, vol. 293, no. 2, pp. H1131–H1137, 2007.

[8] M. Sezgin and B. Sankur, "Survey over image thresholding techniques and quantitative performance evaluation," *J. Elec. Imag.*, vol. 13, no. 1, pp. 146–165, 2004.

[9] V. Caselles, R. Kimmel, and G. Sapiro, "Geodesic active contours," *Int. J. Comp. Vis.*, vol. 22, no. 1, pp. 61–79, 1997.

[10] T. F. Chan and L. A. Vese, "Active contours without edges," *IEEE Trans. Image Processing*, vol. 10, no. 2, pp. 266–277, 2001.

[11] S. K. Nath and K. Palaniappan, "Adaptive robust structure tensors for orientation estimation and image segmentation," *LNCS (ISVC)*, vol. 3804, pp. 445–453, 2005.

[12] F. Bunyak, K. Palaniappan, S. K. Nath, T. I. Baskin, and G. Dong, "Quantitative cell motility for in vitro wound healing using level set-based active contour tracking," in *IEEE ISBI*, 2006, pp. 1040–1043.

[13] I. Ersoy, F. Bunyak, K. Palaniappan, M. Sun, and G. Forgacs, "Cell spreading analysis with directed edge profile-guided level set active contours," *LNCS (MICCAI)*, vol. 5241, pp. 376–383, 2008.

[14] G. Dong and K. Palaniappan, "A robust method for edge-preserving image smoothing," *LNCS (ACIVS)*, vol. 5259, pp. 390–399, 2008.

[15] M. J. Black, G. Sapiro, D. H. Marimont, and D. Heeger, "Robust anisotropic diffusion," *IEEE Trans. Image Processing*, vol. 7, no. 3, pp. 421–432, 1998.

[16] P. Perona and J. Malik, "Scale-space and edge detection using anisotropic diffusion," *IEEE Trans. Pattern Analysis and Machine Intell.*, vol. 12, no. 7, pp. 629–639, 1990.

[17] G. Aubert and P. Kornprobst, *Mathematical problems in image processing: Partial differential equation and calculus of variations*, Springer-Verlag, 2006.

[18] C. Tomasi and R. Manduchi, "Bilateral filtering for gray and color images," in *IEEE ICCV*, 1998, pp. 59–66.

[19] D. Barash, "A fundamental relationship between bilateral filtering, adaptive smoothing, and the nonlinear diffusion equation," *IEEE Trans. Pattern Analysis and Machine Intell.*, vol. 24, no. 6, pp. 844–847, 2002.

[20] V. B. S. Prasath and A. Singh, "Well-posed inhomogeneous nonlinear diffusion scheme for digital image denoising," *J. Appl. Math.*, vol. 2010, 2010.

[21] V. B. S. Prasath and A. Singh, "An adaptive anisotropic diffusion scheme for image restoration and selective smoothing," *Int. J. Image and Graphics*, vol. 12, no. 1, 2012.

[22] W. Niblack, *An Introduction to Digital Image Processing*, Prentice Hall, 1986.

[23] S. K. Nath, K. Palaniappan, and F. Bunyak, "Accurate spatial neighborhood relationships for arbitrarily-shaped objects using Hamilton-Jacobi GVD," *LNCS (SCIA)*, vol. 4522, pp. 421–431, 2007.